Chemical Engineering Journal 460 (2023) 141653

Contents lists available at ScienceDirect

Chemical Engineering Journal

journal homepage: www.elsevier.com/locate/cej

Carbon fibers as additives to engineer agglomeration and propagation of aluminized propellants

Haiyang Wang, Erik Hagen, Keren Shi, Steven Herrera, Feiyu Xu, Michael R. Zachariah *

The University of California Riverside, CA 92521, USA

ARTICLE INFO

Keywords:
Carbon fibers
Solid propellant
Agglomeration
Aluminum

ABSTRACT

A major challenge in the application of aluminum (Al) in solid propellants lies in the incomplete combustion and severe agglomerations of Al particles that cause two-phase flow loss in aluminized solid rocket motor. In this work, 2.5 wt% carbon fibers embedded into Al/AP/HTPB solid propellant shows a ~ 25 % enhancement in burn rate. In-situ microscopic observation and thermal imaging of combustion find that carbon fibers intercept ejected hot agglomerates near the burning surface and enhance heat feedback to the unreacted material. The post-combustion products were also collected and analyzed, confirming that polyacrylonitrile (PAN)-based carbon fibers keeps their integrity during the combustion, thus can efficiently catch the hot agglomerates and promote the heat feedback. This study outlines how these approaches may enhance the propagation and reduce the two-phase flow losses in solid propulsion.

1. Introduction

Aluminum (Al) particles are commonly used in propellants, explosives, and pyrotechnics to increase the energy density of the energetic composites [1–5]. Using nano-sized Al to replace conventional Al microparticles, offer higher energy release rate and a decrease in ignition temperature (1000 K vs 2300 K) [6–9]. However, nano-sized Al particles suffer from high viscosity induced handling issues [10–13] and severe sintering/agglomerating [14–18], which significantly increase the effective Al size (from nm to μm) during combustion, lowering the energy release rate of aluminized energetic composites, and muting the theoretical benefits of going to the nanoscale.

The sintering/agglomerating of micro-sized aluminum (Al) particles has been commonly studied in solid propulsion, which is considered to be a major cause for loss in specific impulse (two-phase loss) and might cancel out the advantages of the addition of nano-Al [19–23]. Commonly, ex-situ techniques such as electron-microscopic characterization on the quenched/captured agglomerates are used to evaluate agglomeration. Recently, in-situ techniques such as time-resolved X-ray imaging [24–28] and digital in-line holography [22,29–32] have been employed to observe the agglomeration and sintering in the combustion of aluminized energetic composites.

Recently, high-speed microscopy has been employed to observe the agglomerating process of nanosized Al particles at high spatial (μm) and temporal (μs) resolution and some approaches to affect agglomeration and flame propagation were proposed [16,33–37]. One approach we found was that addition of carbon fibers can promote the flame propagation and reduce the agglomeration size of Al/CuO nanothermite composite [33]. With the addition of only ~2.5 wt% carbon fibers (CF, the propagation rate of the composite was promoted by > 2x. From *in-operando* microscopic observations, we found that the carbon fibers intercept ejected hot agglomerates from the burning surface which provided enhanced heat feedback to the unburnt materials. In that work, we proposed that the carbon fibers might also enhance the combustion of aluminized propellants in a similar way.

As a follow on then, in this work, carbon fibers were embedded into aluminized propellants, and we observed that the burn rate increases by ~25 % with an addition content of only ~2.5 wt of CF. High-speed macroscopic and microscopic videos also confirm that the carbon fibers "catch" the agglomerates ejecting from the burning surface, providing efficient heat feedback to the unburnt surface and creating a deepened pre-heating zone. In this work, different types of carbon fibers were also compared, with polyacrylonitrile (PAN)-based carbon fibers found to be the most efficient in promoting flame propagation of aluminized propellants due to their better tolerance to high temperatures compared to other types of carbon fibers. This study provides a simple approach to increase the burn rate of aluminized propellants, reduce the agglomerates and two-phase flow losses in solid propulsion.

* Corresponding author at: Department of Chemical and Environmental Engineering, University of California, Riverside, California 92521, United States.
E-mail address: mrz@engr.ucr.edu (M.R. Zachariah).

https://doi.org/10.1016/j.cej.2023.141653
Received 18 December 2022; Received in revised form 13 January 2023; Accepted 29 January 2023
Available online 31 January 2023

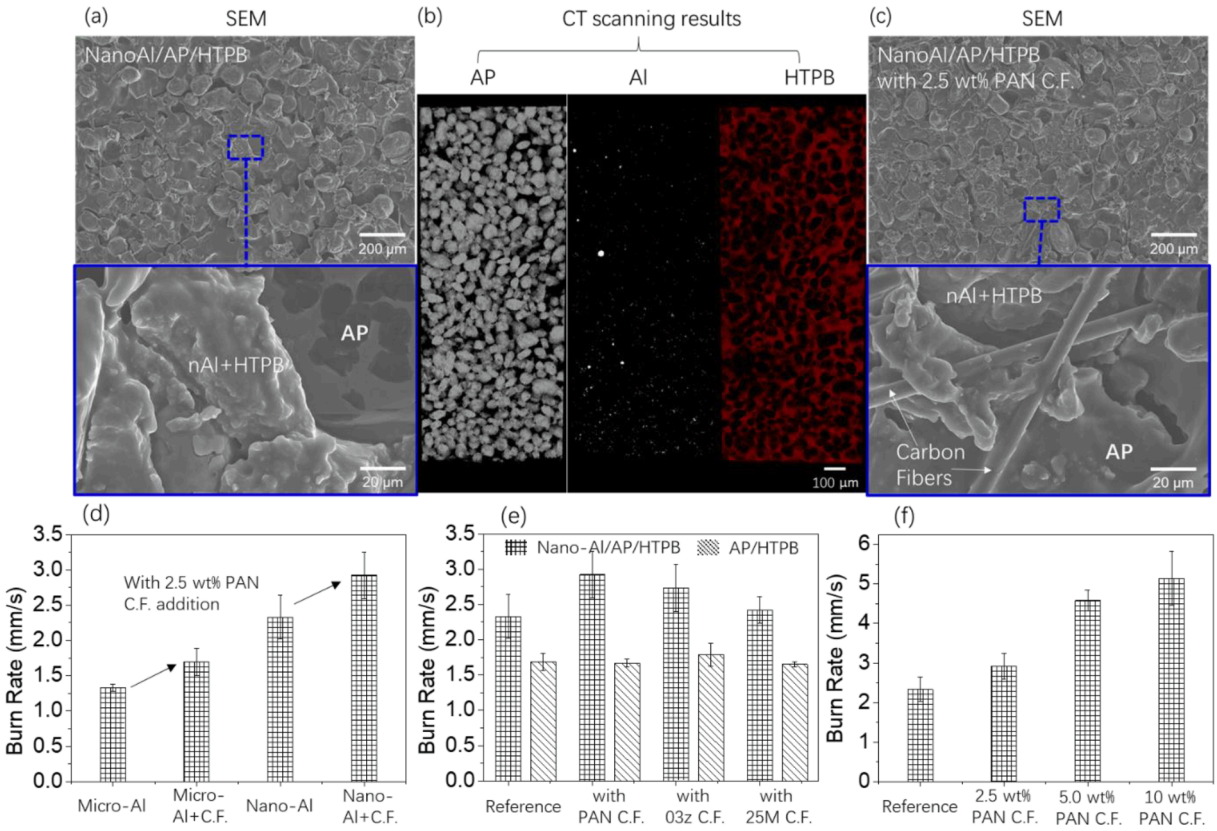

Fig. 1. SEM images (a, and c) and CT scanning images (b) of nanoAl/AP/HTPB with (2.5 wt%) and without PAN-based carbon fibers. Measured burn rates (d) of different Al/AP/HTPB propellant grains (with microsized and nanosized Al) with and without 2.5 wt% PAN-based carbon fiber addition; Measured burn rates (e) of AP/HTPB and Al/AP/HTPB (with nanosized Al) with different carbon fibers addition (2.5 wt% of carbon fibers labelled as PAN, 03z, and 25 M). Measured burn rates (f) of Al/AP/HTPB (with nanosized Al) with different carbon fibers addition from 2.5 wt% to 10 wt%.

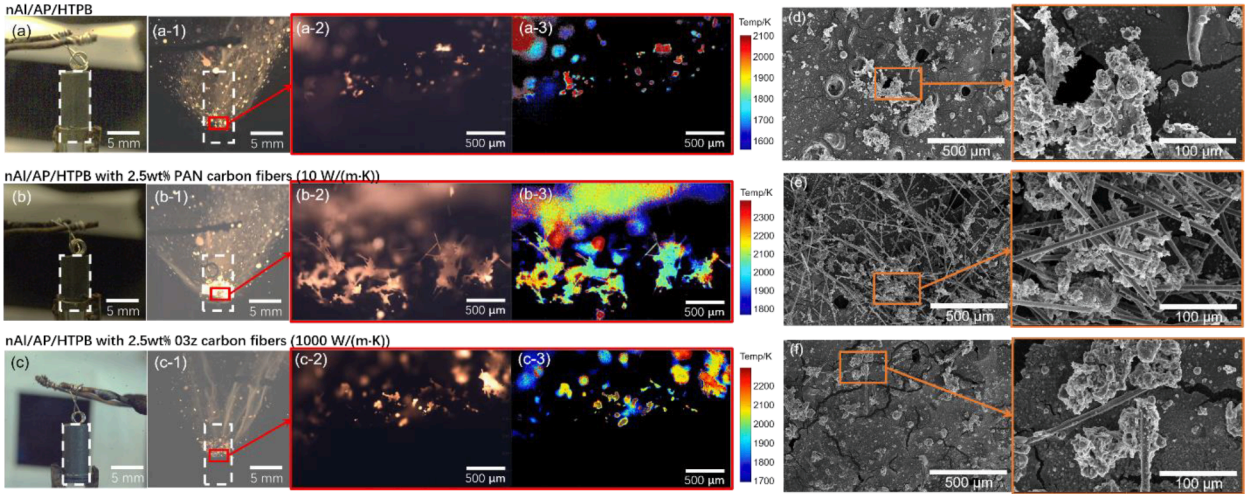

Fig. 2. Macroscopic (a-c) and microscopic (a-1 ~ c-1) burning snapshots, the corresponding microscopic temperature maps (a-2 ~ c-2) of Al/AP/HTPB (Ø=1) solid propellant grain (diameter = 4.7 mm) without carbon fibers (a), with PAN-based (b) and graphite-based (03z) carbon fibers (c). Low and higher magnification SEM images (d-f) of the post-combustion products of Al/AP/HTPB (Ø=1) solid propellants without carbon fibers (d), with PAN-based (e) and graphite-based (03z) carbon fibers (f). Note: carbon fibers' content is ~2.5 wt%.

2. Experimental section

2.1. Materials

Microsized aluminum particles (−100 + 325 mesh, ~50 μm, 99.5 % active content) were purchased from Thermo Scientific. Al nanoparticles (NPs) were purchased from Argonide Corporation with an average size of ~50 nm and an active content of 67 wt% according to thermogravimetric measurement. Ammonium perchlorate (AP) particles (90 μm) were purchased from Pyro. Chem. Source. The scanning electron microscope images of microsized Al, Al NPs and AP microparticles are shown in Fig. S1. Hydroxyl-terminated Polybutadiene (HTPB, OH value

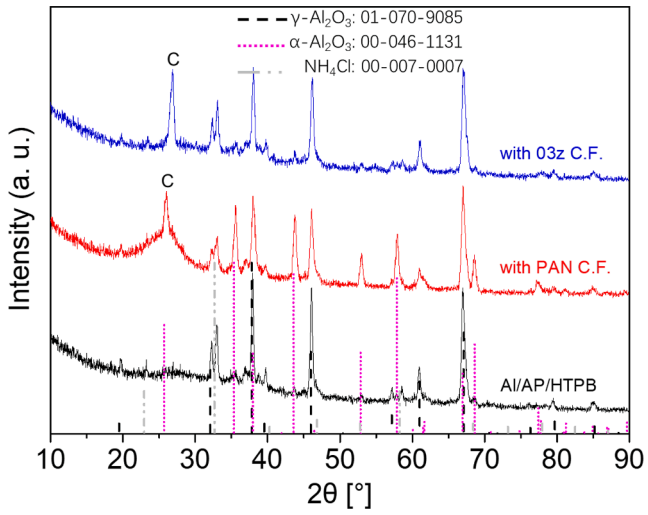

Fig. 3. XRD of the post-combustion products of Al/AP/HTPB (Ø=1) solid propellant without carbon fibers (a, and d), with PAN-based (b, and e) and graphite-based (03z) carbon fibers (c, and f). Note: carbon fibers' content is ~ 2.5 wt%. More α-phase Al_2O_3 in the PAN-based carbon fiber case compared to the other two, further confirming the higher heat feedback.

0.81, measured by the vendor), methylene diphenyl diisocyanate (MDI, modified curing agent), and isodecyl pelargonate (IDP) plasticizer were purchased from Rocket Motor Components, Inc. Polyacrylonitrile (PAN)-based carbon fibers (diameter: 7 μm) were purchased from Composite Envisions, which were chopped in a length of ~3 mm. Highly thermal conductive fibers (graphite fibers with product # of XN-100, diameter: 10 μm) are gifted by Nippon Graphite Fiber Corp. from Japan. Two different graphite fibers were provided with a chopped length of ~3 mm and ~25 μm, which are labeled as 03z and 25 M, respectively. The detailed physical properties (thermal conductivity, density, filament diameter, and length) of the carbon fibers are summarized in Table S1. SEM images of the fibers are shown in Fig. S2.

2.2. Propellant grain preparation

A detailed formulation with weight of each composition can be found in Tables S2. Typically, ~392 mg HTPB was weighed, then ~58 mg MDI and ~ 50 mg IDP were added into the HTPB. The mixture was then mixed for 5 mins at a rate of 2000 rpm in a mixer (Thinky AR100). Then 62.5 mg carbon fibers were added into the above binder mixture and mixed for 10 mins, and 1750 mg AP was added into the above binder and mixed for 10 mins. Finally, 250 mg Al was added and mixed for another 10 mins. In a typical cast process, slurries were pressed using a syringe pump to remove any air. Then the propellant filled syringe was stored in a fume hood for 3 days to fully cure the HTPB. Following this, the solid propellant grain was cut into desired lengths for combustion characterization. The density (mass/volume) was determined from the mass and geometry of each propellant grain rod. The measured and theoretical densities of the propellant grains are summarized in Fig. S3. For preparation of AP/HTPB, all the procedures are the same except the addition of Al NPs.

2.3. SEM/EDS, XRD, TG/DSC and X-ray tomography

The morphologies and compositions of the carbon fibers, the cured propellant grains, and the post-combustion products were characterized by scanning electron microscope (SEM, Thermo-Fisher Scientific NNS450) coupled with energy dispersive X-ray spectroscopy (EDS). The post-combustion products were also characterized by X-ray Powder Diffraction (XRD, PANalytical Empyrean Series 2). Thermogravimetric analysis/differential thermal analysis (TGA/DSC, Proteus80 from NETZSCH) in this study were conducted in argon flow (50 mL/min) at a heating rate of 10 °C/min from room temperature to 425 °C. X-ray tomography was performed using the Zeiss Versa 510 (UCSD NCMIR). The sample was scanned as printed on a glass slide. The X-ray source was operated at 80 kV and 75 μA with a LE1 filter inserted. The source distance and a detector distance, 41000 mm and 19000 mm respectively, with a 4x objective contributed to a pixel size of 4.7 μm. Exposure time for each projection was 1.5 *sec*.

2.4. Macroscopic and microscopic imaging

The experimental setup used in this study is shown in Fig. S4. The samples are solid propellant grains (~1 cm long, ~4.7 mm in diameter). The propellant grains were ignited by nichrome wire in open air (1 atm). One high-speed camera (Vision Research Phantom Miro M110) captures the macroscopic combustion of the grain at a sample rate of 1,500 frames/s (832 × 800 pixels), while a microscopic imaging system (~2.2 μm/pixel, Vision Research Phantom VEO710L coupled to Infinity Photo-Optical Model K2 DistaMax) captures the microscopic combustion at a sample rate of 7,500 frames/s (1280 × 800 pixels).

2.5. Burn rate and flame temperature measurement

The burn rates (ν) of the propellant grains were determined from the macroscopic ***deos. Burn rate was calculated by dividing the length of the sample (1 cm) by the burn time observed with the macroscopic ***deo. Average burn rates of triplicate experiments for each sample are reported with standard deviation. The burn rate data was also further confirmed by a setup (Fig. S5a) using a linear variable differential transformer (LVDT, displacement sensor purchased from Omega) as described in other studies [38,39]. The comparison using different burn rate measurement methods are shown in Fig. S5b and S5c. The details of color pyrometry are in our previous studies [36,40]. Briefly, three channel intensity (red, green, blue) ratios are extracted, processed, and demosaiced for the camera's Bayer filter (MATLAB). The system was calibrated with a blackbody source (Mikron, Oriel) and the temperature uncertainty is estimated to be ~200–300 K.

2.6. Infrared radiation (IR) measurement of the pre-heating zones

The IR measurement setup used in this study is shown in Fig. S6. The Al/AP/HTPB (with Al NPs) with (with PAN-based and 03z carbon fibers) and without carbon fibers (reference) were casted on thin silicon wafers (thickness: 75 μm). The propellant films thickness is ~1 mm. The IR camera (Telops FAST M3K high-speed infrared camera) captured the infrared radiation signals through the silicon wafers. The lens used in this study is G4x microscope lens (Telops), and have a resolution of ~10 μm/pixel. The transmittance of the silicon wafer is 55 % in the spectral range of the IR camera (3–5 μm) (Thermo Scientific FT-IR Spectrometer Nicolet iS50).

2.7. Post-combustion products analysis

The post-combustion products of the solid propellants: Al/AP/HTPB (with Al NPs) with (with PAN-based and 03z carbon fibers) and without carbon fibers (reference) were collected as shown in Fig. S7a and S7b, for SEM/EDS (Fig. S8) and XRD (Fig. S9) characterization, respectively.

3. Results and discussions

3.1. Embedding carbon fibers into Al/AP/HTPB

The solid propellant grains were prepared by casting and curing the composite in a syringe with an inner diameter of 4.7 mm. The SEM and CT scanning images of Al/AP/HTPB grains are shown in Fig. 1a and Fig. 1b, respectively, which confirms the close and uniform packing of

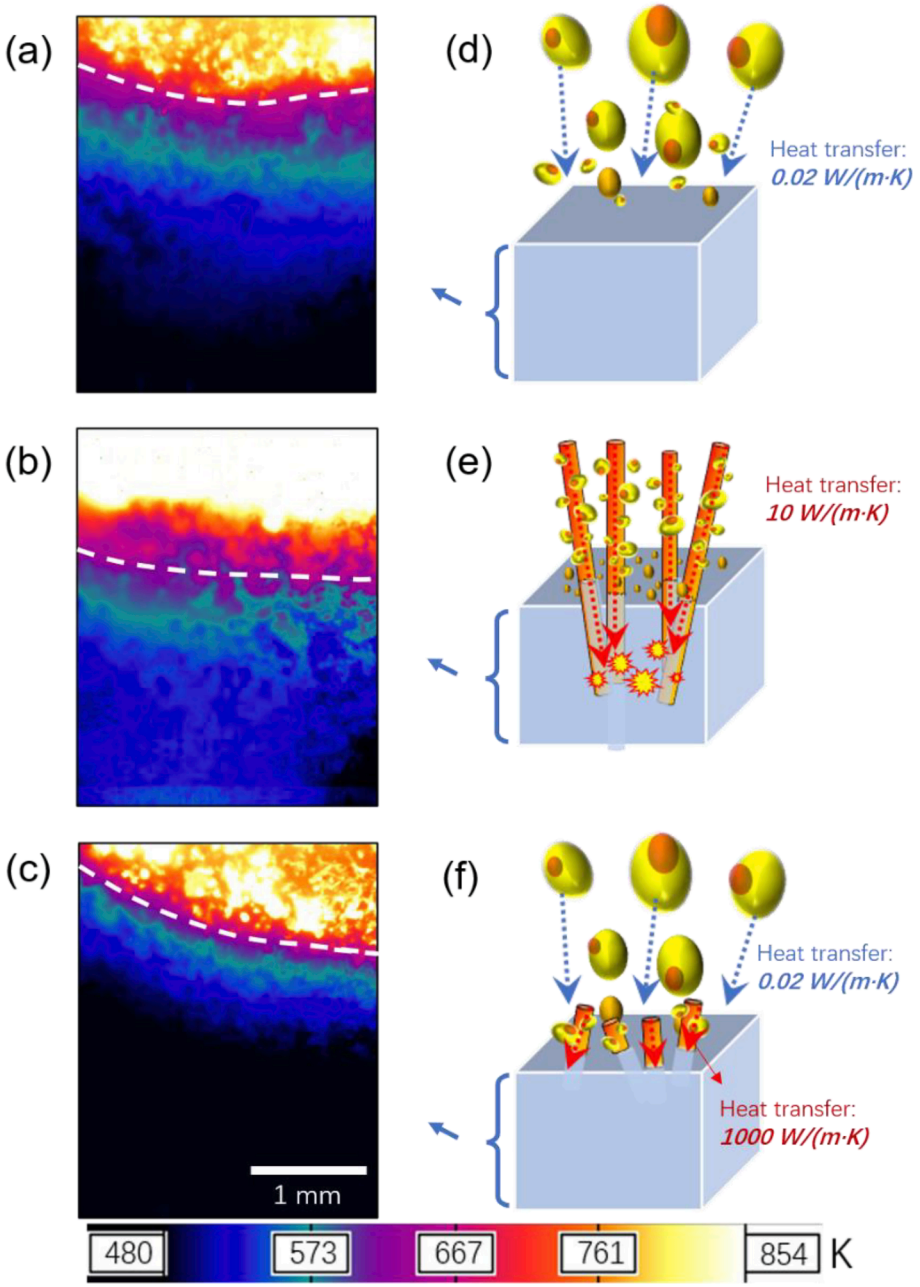

Fig. 4. IR measurement on the pre-heating areas (a-c) and schematic showing (a-c) of the heat feedback (d-f) of Al/AP/HTPB (Ø=1) solid propellant without carbon fibers (a, and d), with PAN-based (b, and e) and graphite-based (03z) carbon fibers (c, and f). The propellants are pre-cast on a thin silicon wafer (75 μm) with a thickness of ~1 mm, and the IR measurements are looking through the wafer. Note: white dash lines (a-c) indicate the burning surface.

AP particles (mean size 90 μm) in an Al/HTPB matrix. The carbon fibers (PAN-based) embedded in Al/AP/HTPB (with 2.5 wt% carbon fibers) are observed in Fig. 1c.

All the solid propellant grains were ignited by nichrome wires in the air (1 atm) and the burning rates (Fig. 1d–f) are obtained via high-speed videos (supporting videos). As Fig. 1d shows, the burn rates of solid propellant grains are increased by ~28 % and ~25 % with 2.5 wt% addition of carbon fibers, for micro-sized Al and nano-sized Al based solid propellants, respectively. Different carbon fibers (details about different carbon fibers are shown in Fig. S2 and Table S2) were also added into Al/AP/HTPB (with nanosized Al) and AP/HTPB (with no Al) grains. As shown in Fig. 1e, all types of carbon fibers increased the burn rates of Al/AP/HTPB to different, while no effects were observed on the burn rates of AP/HTPB without Al. Among different types of carbon fibers, the PAN-based carbon fibers (thermal conductivity 10 W/(m·K), length 3 mm) are the most efficient, followed by the graphite-based carbon fibers (03z, thermal conductivity > 900 W/(m·K), length 3 mm), and the shorter version (25 M, thermal conductivity > 900 W/(m·K), length 0.25 mm) of the former graphite-based carbon fibers. Fig. 1e indicates the enhancement of burn rates cannot be attributed to thermal transport into the solid propellant as there is no observed effect with the addition of higher thermally conductive carbon fibers. Different PAN-based carbon fibers from 2.5 wt% to 10 wt% were added into Al/AP/HTPB (with nanosized Al). As Fig. 1f shows, the burn rates increased with the carbon fibers content, further confirms the enhancement. It is noted that there is an abrupt increase (>50 %) on the burn rate when the carbon fiber content increased from 2.5 wt% to 5 wt%, and likely because of the packing density is reduced from ~ 100 % to ~ 84 % (Fig. S3).

As we mentioned above, our previous work with added carbon fibers

to Al/CuO thermite composites observed carbon fibers "catching" the agglomerates of Al and thus having an efficient means to couple heat back to the sold composite, [33]. In this study, we embedded carbon fibers into Al/AP/HTPB propellants and the agglomeration status of Al NPs were observed via a dual-camera (macroscopic and microscopic high-speed cameras) system (Fig. S4). As the macroscopic video snapshots (Fig. 2a–c) show, the propellant with PAN-based carbon fibers has much thicker and brighter flame front compared to the other two cases. After zooming in, the microscopic video snapshots (Fig. 2a-1 ~ 2c-1) and the corresponding pyrometry results (Fig. 2a-2 ~ 2c-2) confirm that the agglomerates formed from Al NPs were caught by the carbon fibers and burned closer to the surface of propellant, providing more heat feedback to the unburnt materials.

Even though both carbon fibers (PAN and graphite based) intercept the agglomerates, the PAN-based carbon fibers in the flame are much longer compared to the graphite-based carbon fibers during the combustion, indicating PAN-based carbon fibers survived better at high temperature (Fig. 2a–c and supporting videos). The post-combustion products were collected and the SEM/EDS images are shown in Fig. 2d–f and Fig. S8, respectively, which confirm that PAN-based carbon fibers survive in the combustion while graphite-based carbon fibers break into much shorter ones (<0.1–0.5 mm) as compared to their original length (~3 mm). Graphite-based carbon fibers may break due to defects containing functional groups that when heated result in delamination and thus breakage. This would require further investigation. Fig. 2 and Fig. S8 also confirm that the agglomerates were caught by the carbon fibers and their relatively smaller agglomeration size compared to the reference (no carbon fiber case).

The XRD results (Fig. 3) of the post-combustion products show that significantly higher amount of α-phase Al_2O_3 was detected in the PAN-based carbon fiber case compared to the other two, further confirming the higher heat feedback as the transition from γ-phase Al_2O_3 to α-phase Al_2O_3 requires higher temperature and longer residence time [41,42].

The above-mentioned heat feedback was further confirmed by IR measurement on the pre-heating zones of the solid propellants, which are shown in Fig. 4a–c at the temperature range of 480–854 K. The calculated head flux at the burning surface by the tangent line shows ~ 36 % increase in the propellant with the PAN-based carbon fibers while the addition of 03z carbon fibers only increase the heat flux by ~18 % (Table S3)[43]. The PAN-based carbon fiber case has the largest pre-heating zone, confirming more efficient heat feedback (Fig. 4b). In contrast, the TG/DSC results (Fig. S9) show that all three samples (reference, PAN-based and graphite based) have roughly the same decomposition stages of AP, confirming no chemical effects from the addition of carbon fibers.

Clearly, the PAN-based carbon fiber case has the largest pre-heating zone, confirming more efficient heat feedback (Fig. 4b). In the contrast, the TG/DSC results (Fig. S9) show that all the three samples (reference, PAN-based case, and graphite-based case) have the roughly same decomposition stages of AP, confirming no chemical effects from carbon fiber addition.

As proposed in Fig. 4d–f, the heat feedback from the flame to the burning surface is enhanced due to the addition of carbon fibers. Clearly, PAN-based carbon fibers (10 W/(m·K)) provide for faster heat transfer routes from the flame to the unburnt material compared to only gas phase conduction (0.02 W/(m·K)). However, the enhancement from the graphite-based carbon fibers (~1000 W/(m·K)) is likely not relevant due to many of the fibers burning and not sticking out far enough from the burning surface, making the agglomerate "catching" ability much lower. Therefore, even though the heat conductivity of graphite-based carbon fibers is ~10x higher than the PAN-based carbon fibers, the enhancement on the flame propagation of Al/AP/HTPB is not further increased (Fig. 1e).

4. Conclusion

In this work, carbon fibers were embedded into aluminized propellants and were found to increase the burn rate by ~25 % with the addition ~2.5 wt% CF. High-speed macroscopic and microscopic videos show that the carbon fibers intercept the agglomerates ejecting from the burning surface, providing more heat feedback to the unburnt surface and creating a deeper pre-heating zones, which are confirmed by the diffusion analysis (post-combustion product) and infrared thermal measurement (pre-heating areas). Different types of carbon fibers were compared and the PAN-based carbon fibers were found to be the most efficient to promote flame propagation of aluminized propellants. The PAN-based carbon fibers can survive the flame and retains their integrity, confirmed by the electron microscopy characterization on the post-combustion products. This study provides a simple approach to increase the burn rate of aluminized propellants, reduce the agglomerates and two-phase flow losses in solid propulsion.

Author Contributions

M. R. Z initiated and supervised the research. H. W. prepared the propellants grains and carried out the characterization, combustion measurements, and analysis. E. H. designed and manufactured the LVDT-based system. K. S. conducted and analyzed the IR measurement of the propellant burning. S. H. conducted and analyzed the CT scanning of the propellant grains. F. X. conducted the XRD characterization of the post-combustion products. H. W. prepared the manuscript and all the authors made comments on the manuscript. All authors have given approval to the final version of the manuscript.

Declaration of Competing Interest

The authors declare that they have no known competing financial interests or personal relationships that could have appeared to influence the work reported in this paper.

Data availability

Data will be made available on request.

Acknowledgements

We gratefully acknowledge support from AFOSR and ARO. We also thank the CFAMM at the University of California, Riverside, for their microscopy support. We thank Tao Wu and Prof. Carole Rossi from LAAS-CNRS for gifting us the silicon wafers.

Appendix A. Supplementary data

SEM images of Al and AP particles, as well as different types of carbon fibers. Physical properties of different types of carbon fibers, as well as the detailed formulations of the solid propellants used in this study. The measured and theoretical densities of different Al/AP/HTPB propellant grains used in this study. Macroscopic and microscopic imaging, as well as the IR systems for the solid propellant grain burning. Setup for using a LVTD based burn rate measuring and setup for the post-combustion products collecting. The SEM/EDS of the post-combustion products. The TG/DSC results of Al/AP/HTPB grains with different types of carbo fibers. **Video 1**: macroscopic burning videos of microAl-AP-HTPB with and without 2.5 % PAN-based carbon fibers. **Video 2**: macroscopic burning videos of nanoAl-AP-HTPB with and without 2.5 % PAN-based carbon fibers. **Video 3**: macroscopic burning videos of nanoAl-AP-HTPB with 2.5 % different types of carbon fibers (PAN, 03z, and 25 M). **Video 4**: microscopic burning videos of nanoAl-AP-HTPB with 2.5 % different types of carbon fibers (PAN, 03z, and 25 M). **Video 5**: microscopic burning videos with pyrometry of nanoAl-AP-HTPB with 2.5 % different types of carbon fibers (PAN, 03z, and 25 M). **Video 6**: macroscopic burning videos of nanoAl-AP-HTPB with

different addition content of carbon fibers (from 2.5 wt% to 10 wt%). **Video 7:** macroscopic burning videos of AP-HTPB with 2.5 % different types of carbon fibers (PAN, 03z, and 25 M). Supplementary data to this article can be found online at https://doi.org/10.1016/j.cej.2023.141653.

References

[1] E.L. Dreizin, Metal-based reactive nanomaterials, Prog. Energy Combust. Sci. 35 (2) (2009) 141–167, https://doi.org/10.1016/j.pecs.2008.09.001.

[2] R.A. Yetter, G.A. Risha, S.F. Son, Metal particle combustion and nanotechnology, Proc. Combust. Inst. 32 (2) (2009) 1819–1838, https://doi.org/10.1016/j.proci.2008.08.013.

[3] M. Örnek, K.E. Uhlenhake, Y. Zhou, B. Zhang, M. Kalaswad, D.N. Collard, H. Wang, Q. Wang, S.F. Son, Preparation and characterization of multifunctional piezoenergetic polyvinylidene fluoride/aluminum nanocomposite films, J. Appl. Phys. 131 (5) (2022), 055108, https://doi.org/10.1063/5.0076258.

[4] W. Cao, J. Ran, H. Wang, W. Guo, X. Lu, J. Wang, Energy performance of hmx-based aluminized explosives containing polytetrafluoroethylene (PTFE), Propellants Explos. Pyrotech. 47 (6) (2022), https://doi.org/10.1002/prep.202200004.

[5] Y. Zhu, W. Le, W. Zhao, X. Ma, D. Liu, J. Li, Q. Jiao, Promising fuels for energetics: spherical al-li powders with high reactivity via incorporation of Li, Fuel 323 (2022), 124393, https://doi.org/10.1016/j.fuel.2022.124393.

[6] D.S. Sundaram, P. Puri, V. Yang, A general theory of ignition and combustion of nano- and micron-sized aluminum particles, Combust. Flame 169 (2016) 94–109, https://doi.org/10.1016/j.combustflame.2016.04.005.

[7] J. Wang, Y. Qu, F. Gong, J. Shen, L. Zhang, A promising strategy to obtain high energy output and combustion properties by self-activation of nano-Al, Combust. Flame 204 (2019) 220–226, https://doi.org/10.1016/j.combustflame.2019.03.016.

[8] K.J. Kim, M.H. Cho, S.H. Kim, Effect of aluminum micro- and nanoparticles on ignition and combustion properties of energetic composites for interfacial bonding of metallic substrates, Combust. Flame 197 (2018) 319–327, https://doi.org/10.1016/j.combustflame.2018.08.016.

[9] M. Lucas, S.J. Brotton, A. Min, C. Woodruff, M.L. Pantoya, R.I. Kaiser, Effects of size and prestressing of aluminum particles on the oxidation of levitatedexo -tetrahydrodicyclopentadiene droplets, J. Phys. Chem. A 124 (8) (2020) 1489–1507, https://doi.org/10.1021/acs.jpca.9b10697.

[10] L.T. DeLuca, Overview of al-based nanoenergetic ingredients for solid rocket propulsion, Def. Technol. 14 (5) (2018) 357–365, https://doi.org/10.1016/j.dt.2018.06.005.

[11] H. Wang, G. Jian, S. Yan, J.B. DeLisio, C. Huang, M.R. Zachariah, Electrospray formation of gelled nano-aluminum microspheres with superior reactivity, ACS Appl. Mater. Interfaces 5 (15) (2013) 6797–6801, https://doi.org/10.1021/am401238t.

[12] F. Maggi, Curing viscosity of htpb-based binder embedding micro- and nano-aluminum particles, Propellants Explos. Pyrotech. 39 (5) (2014) 755–760, https://doi.org/10.1002/prep.201400010.

[13] F.D. Ruz-Nuglo, L.J. Groven, 3-D printing and development of fluoropolymer based reactive inks, Adv. Eng. Mater. 20 (2) (2018) 1700390, https://doi.org/10.1002/adem.201700390.

[14] Q. Chu, X. Chang, D. Chen, A physiochemical model for the combustion of aluminum nano-agglomerates in high-speed flows, Combust. Flame (2021), 111739, https://doi.org/10.1016/j.combustflame.2021.111739.

[15] L.T. De Luca, L. Galfetti, F. Severini, L. Meda, G. Marra, A.B. Vorozhtsov, V. S. Sedoi, V.A. Babuk, Burning of nano-aluminized composite rocket propellants, Combust. Explos. Shock Waves 41 (6) (2005) 680–692, https://doi.org/10.1007/s10573-005-0080-5.

[16] H. Wang, D.J. Kline, P. Biswas, M.R. Zachariah, Connecting agglomeration and burn rate in a thermite reaction: role of oxidizer morphology, Combust. Flame 231 (2021), 111492, https://doi.org/10.1016/j.combustflame.2021.111492.

[17] V.S. Parimi, S. Huang, X. Zheng, Enhancing ignition and combustion of micron-sized aluminum by adding porous silicon, Proc. Combust. Inst. 36 (2) (2017) 2317–2324, https://doi.org/10.1016/j.proci.2016.06.185.

[18] L. Galfetti, L.T. DeLuca, F. Severini, G. Colombo, L. Meda, G. Marra, Pre and post-burning analysis of nano-aluminized solid rocket propellants, Aerosp. Sci. Technol. 11 (1) (2007) 26–32, https://doi.org/10.1016/j.ast.2006.08.005.

[19] K. Tejasvi, V. Venkateshwara Rao, Y. Pydi Setty, K. Jayaraman, Ultra-fine aluminium characterization and its agglomeration features in solid propellant combustion for various quenched distance and pressure, Propellants Explos. Pyrotech. 45 (5) (2020) 714–723, https://doi.org/10.1002/prep.201900371.

[20] K. Tejasvi, V. Venkateshwara Rao, Y. PydiSetty, K. Jayaraman, Studies on aluminum agglomeration and combustion in catalyzed composite propellants, Combust. Explos. Shock Waves 57 (2) (2021) 203–214, https://doi.org/10.1134/S001050822102009X.

[21] L.T. DeLuca, L. Galfetti, G. Colombo, F. Maggi, A. Bandera, V.A. Babuk, V. P. Sinditskii, Microstructure effects in aluminized solid rocket propellants, J. Propuls. Power 26 (4) (2010) 724–732, https://doi.org/10.2514/1.45262.

[22] B. Sha, X. Na, Z. Xia, X. Yan, Y. Li, Y. Feng, Y. Zi, Analysis of agglomeration particle size near the burning surface of aluminized solid propellant based on digital inline holography, Acta Astronaut. 188 (2021) 140–150, https://doi.org/10.1016/j.actaastro.2021.07.015.

[23] W. Ao, Z. Fan, L. Liu, Y. An, J. Ren, M. Zhao, P. Liu, L.K.B. Li, Agglomeration and combustion characteristics of solid composite propellants containing aluminum-based alloys, Combust. Flame 220 (2020) 288–297, https://doi.org/10.1016/j.combustflame.2020.07.004.

[24] D.N. Collard, M.S. McClain, N.A. Rahman, N.H. Dorcy, T.R. Meyer, S.F. Son, Dynamic x-ray imaging of additively manufactured reactive components in solid propellants, J. Propuls. Power 37 (3) (2021) 362–368, https://doi.org/10.2514/1.B38128.

[25] J. Kalman, A.R. Demko, B. Varghese, K.E. Matusik, A.L. Kastengren, Synchrotron-based measurement of aluminum agglomerates at motor conditions, Combust. Flame 196 (2018) 144–146, https://doi.org/10.1016/j.combustflame.2018.06.013.

[26] M.D. Grapes, R.V. Reeves, K. Fezzaa, T. Sun, J.M. Densmore, K.T. Sullivan, In situ observations of reacting al/fe2o3 thermite: relating dynamic particle size to macroscopic burn time, Combust. Flame 201 (2019) 252–263, https://doi.org/10.1016/j.combustflame.2018.12.021.

[27] E.R. Wainwright, S.V. Lakshman, A.F.T. Leong, A.H. Kinsey, J.D. Gibbins, S. Q. Arlington, T. Sun, K. Fezzaa, T.C. Hufnagel, T.P. Weihs, Viewing internal bubbling and microexplosions in combusting metal particles via x-ray phase contrast imaging, Combust. Flame 199 (2019) 194–203, https://doi.org/10.1016/j.combustflame.2018.10.019.

[28] D. Stamatis, E.R. Wainwright, S. Vummidi Lakshman, M.S. Kessler, T.P. Weihs, Combustion of explosively dispersed al-mg-zr composite particles, Combust. Flame 217 (2020) 93–102, https://doi.org/10.1016/j.combustflame.2020.03.012.

[29] Y. Wu, Z. Lin, Z. Zhuo, S. Wu, C. Zhou, L. Yao, W. Ao, X. Wu, L. Chen, K. Cen, Particle burning behaviors of al/ap propellant with high-speed digital off-axis holography, Proc. Combust. Inst. 38 (3) (2021) 4401–4408, https://doi.org/10.1016/j.proci.2020.07.135.

[30] A.W. Marsh, G.T. Wang, J.D. Heyborne, D.R. Guildenbecher, Y.C. Mazumdar, Time-resolved size, velocity, and temperature statistics of aluminum combustion in solid rocket propellants, Proc. Combust. Inst. 38 (3) (2021) 4417–4424, https://doi.org/10.1016/j.proci.2020.08.010.

[31] B. Jin, Z. Wang, G. Xu, W. Ao, P. Liu, Three-dimensional spatial distributions of agglomerated particles on and near the burning surface of aluminized solid propellant using morphological digital in-line holography, Aerosp. Sci. Technol. 106 (2020), 106066, https://doi.org/10.1016/j.ast.2020.106066.

[32] Y. Chen, D.R. Guildenbecher, K.N.G. Hoffmeister, M.A. Cooper, H.L. Stauffacher, M.S. Oliver, E.B. Washburn, Study of aluminum particle combustion in solid propellant plumes using digital in-line holography and imaging pyrometry, Combust. Flame 182 (2017) 225–237, https://doi.org/10.1016/j.combustflame.2017.04.016.

[33] H. Wang, D.J. Kline, M.C. Rehwoldt, M.R. Zachariah, Carbon fibers enhance the propagation of high loading nanothermites: in situ observation of microscopic combustion, ACS Appl. Mater. Interfaces 13 (26) (2021) 30504–30511.

[34] T. Wu, B. Julien, H. Wang, S. Pelloquin, A. Esteve, M.R. Zachariah, C. Rossi, Engineered porosity-induced burn rate enhancement in dense al/cuo nanothermites, ACS Appl. Energy Mater. 5 (3) (2022) 3189–3198, https://doi.org/10.1021/acsaem.1c03805.

[35] H. Wang, P. Biswas, D.J. Kline, M.R. Zachariah, Flame stand-off effects on propagation of 3d printed 94 wt% nanosized pyrolants loading composites, Chem. Eng. J. 434 (2022), 134487, https://doi.org/10.1016/j.cej.2021.134487.

[36] D.J. Kline, M.C. Rehwoldt, J.B. DeLisio, S.C. Barron, H. Wang, Z. Alibay, J. C. Rodriguez, G.M. Fritz, M.R. Zachariah, In-operando thermophysical properties and kinetics measurements of al-zr-c composites, Combust. Flame 228 (2021) 250–258, https://doi.org/10.1016/j.combustflame.2020.12.045.

[37] H. Wang, B. Julien, D.J. Kline, Z. Alibay, M.C. Rehwoldt, C. Rossi, M.R. Zachariah, Probing the reaction zone of nanolaminates at ~μs time and ~μm spatial resolution, J. Phys. Chem. C 124 (25) (2020) 13679–13687, https://doi.org/10.1021/acs.jpcc.0c01647.

[38] G. Young, S. Hromisin, S. Loeffler, T.L. Connell, Effect of oxidizer type on solid fuel combustion, J. Propuls. Power 36 (2) (2020) 248–255, https://doi.org/10.2514/1.B37561.

[39] Lee, J. G.; Weismiller, M.; Connell, T. L.; Risha, G. A.; Yetter, R. A.; Gilbert, P. D.; Son, S. F. Ammonia Borane Based-Propellants ER -, 2008.

[40] R.J. Jacob, D.J. Kline, M.R. Zachariah, High speed 2-dimensional temperature measurements of nanothermite composites: probing thermal vs gas generation effects, J. Appl. Phys. 123 (11) (2018), 115902, https://doi.org/10.1063/1.5021890.

[41] M.A. Trunov, M. Schoenitz, X. Zhu, E.L. Dreizin, Effect of polymorphic phase transformations in al2o3 film on oxidation kinetics of aluminum powders, Combust. Flame 140 (4) (2005) 310–318, https://doi.org/10.1016/j.combustflame.2004.10.010.

[42] C. Shen, S. Yan, J. Yao, S. Li, X. Guo, J. Nie, Y. Ou, Q. Jiao, Combustion behavior of composite solid propellant reinforced with al-based alloy fuel, Mater. Lett. 304 (2021), 130608, https://doi.org/10.1016/j.matlet.2021.130608.

[43] K.K. Kuo, R. Acharya (Eds.), Applications of Turbulent and Multiphase Combustion, Wiley, 2012, pp. 1–71.